

Article

Integrating Embedded Discrete Fracture and Dual-Porosity, Dual-Permeability Methods to Simulate Fluid Flow in Shale Oil Reservoirs

Weirong Li ^{1,*}, Zhenzhen Dong ^{2,*} and Gang Lei ^{1,*}

¹ Beijing Innovation Center for Engineering Science and Advanced Technology (BIC-ESAT), Peking University, Beijing 100193, China

² Petroleum Department, Xi'an Shiyou University, Xi'an 710065, China

* Correspondence: liweirong08@gmail.com (W.L.); dongzhenzhen1120@hotmail.com (Z.D.); lg1987cup@126.com (G.L.)

Received: 8 August 2017; Accepted: 18 September 2017; Published: 23 September 2017

Abstract: The oil recovery factor from shale oil remains low, about 5 to 7% of the oil in place. How to increase oil recovery from shale oil reservoirs is attracting more and more attention. CO₂ huff-and-puff was historically considered one of the best approaches to improve the oil rate. Most previous simulation studies have been based on dual porosity, but simulation results from dual-porosity models have not been as accurate as discrete fracture models in composition modeling. This study proposes a new model that integrates the embedded discrete fracture model and the dual-porosity, dual-permeability model (DPDP). The newly developed method could explicitly describe large-scale fractures as flow conduits by embedded discrete fracture modeling and could model the flow in small- and medium-length fractures by DPDP modeling. In this paper, we first introduce four different non-neighboring connections and the way to calculate the transmissibility among different media in the new model. Then, the paper compares the performance of the new method, discrete fracture modeling, DPDP modeling, and embedded discrete fracture modeling for production from oil reservoirs. Following, the paper carries out a series of simulations to analyze the effects of hydraulic fracture stages, hydraulic fracture permeabilities, and natural fracture permeabilities on the CO₂ huff-and-puff process based on the new method. In addition, the injection cycle and soaking time are investigated to optimize CO₂ huff-and-puff performance. This study is the first to integrate embedded discrete fracture modeling with DPDP modeling to simulate the CO₂ huff-and-puff process in a shale oil reservoir with natural fractures. This paper also provides detailed discussions and comparisons on the integrated strategy, embedded discrete fracture modeling, discrete fracture modeling, and dual-porosity, dual-permeability modeling in the context of fracture simulation with a compositional model. Most importantly, this study answers the question regarding how fractures affect CO₂ huff-and-puff and how to optimize the CO₂ huff-and-puff process in a reservoir with natural fractures.

Keywords: CO₂ huff-and-puff; embedded discrete fracture model (EDFM); dual porosity model; shale gas

1. Introduction

Complex fracture networks in shale oil reservoirs make the accurate modeling of oil production in these reservoirs very challenging. Three classes of models, equivalent continuum models (ECMs), dual-continuum models, and discrete fracture models (DFMs) are applied to model fractured systems.

Based on the equivalent continuum theory, Snow [1] first proposed the ECM which describes flow in fractured media mathematically. Since the introduction of this model, several scholars have conducted research on this method, such as Oda [2] and Tian [3].

Dual-continuum modeling is the conventional method for simulating fractured reservoirs and is widely used in the industry. In the 1960s, Barenblatt et al. [4] first established dual-porosity model to simulate matrix-fracture flow systems. Afterward, Warren and Root [5] developed a more complete dual-porosity model. Kazemi et al. [6] and Saidi [7] developed dual-porosity simulators, which extended the Warren and Root approach to multiphase flow. Recently, Pruess and Narasimhan [8] subdivided matrix rock gridding and proposed a multiple interacting continua (MINC) model in 1985. Furthermore, Moinfar et al. [9] proved that the dual-continuum model could not provide accurate solutions in the high-localized anisotropy and presence of large-scale fractures in 2012.

The DFM method, in which an element and a control volume explicitly represents each fracture by, was established to model fluid flow in individual fractures and provide more realistic representations of fractured reservoirs than dual-continuum models. Most DFMs honor the geometry and the location of fracture networks with relying on unstructured grids. Kim and Deo [10] adopted a finite element method to perform discretization for DFM and to combine matrix and fractures based on the superposition principle. Later, Karimi-Fard and Firoozabadi [11] applied DFM to solve the two-phase flow problem in the fractured media. Likewise, Monteagudo and Firoozabadi [12] and Matthäi and Belayneh [13] used control-volume finite element methods for multiphase flow in fractured media and developed numerical simulators. Karimi-Fard et al. [14] extended DFMs compatible with multiphase reservoir simulators based on an unstructured control-volume finite difference formulation. In addition, Li and Lee [15] and Moinfar et al. [9] developed embedded discrete fracture models (EDFMs), which use a structured grid to represent the matrix and introduce additional fracture control volumes by computing the intersection of fractures with the matrix grid. Recently, more attention is paid to the EDFM because of its flexibility and accuracy. Hadi Hajibeygi et al. [16] proposed the iterative multiscale finite volume (i-MSFV) approach to improve the efficiency and the accuracy for fractured porous media, and the results are very promising. Tene et al. [17] proposed a projection-based EDFM to deal with cases where the fracture permeability lies below that of the matrix. The fracture-crossflow-equilibrium method was proposed in 2017 by Ali Zidane and Abbas Firoozabadi [18] to study compositional two-phase flow in the fractured media; simulation results showed that central processing unit (CPU) time with fractured media and without fractured media differs by less than a factor of two. Sander Plumiers [19] introduced hierarchical fracture modeling (HFM) in 2015, upscaling small- and medium-scale fractures into an effective matrix permeability and studying upscaling criteria for the HFM.

In order to balance accuracy, computational efficiency, and field practice, we propose a new method that integrates EDFM and dual-porosity, dual-permeability (DPDP) concepts to model the production process in shale oil reservoirs. The developed method could explicitly describe large-scale permeable fractures as flow conduits and simulate natural fracture networks that connect the global flow in stimulated areas of shale oil reservoirs. It may take years to reach the pseudo-steady state in the matrix systems, so the traditional dual-porosity approach can result in large inaccuracies. With the newly developed simulator, we perform comprehensive simulation studies to determine the key factors of fractures and reservoir which affect the ultimate oil recovery in shale oil reservoirs. Different engineering factors and injection strategies are also analyzed and compared to provide guidance for production optimization during the CO₂ huff-and-puff process.

2. Methodology

Naturally fractured reservoirs typically have a wide range of fracture length-scales, ranging from micrometers up to several hundred meters. Figure 1 shows the correlation between fracture density and length. The small- to medium-scale fractures usually have higher densities than large-scale fractures in the reservoir. These fractured reservoirs are geologically too complex to be fully represented by a DFM because it individually represents each fracture.

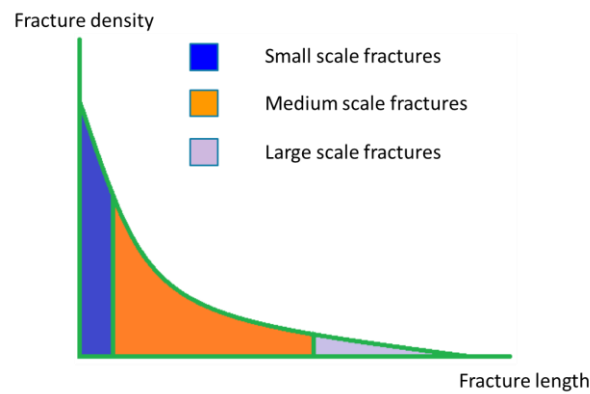


Figure 1. Fracture density and fracture length correlation.

Therefore, a new model is developed combining the EDFM with the DPDP model to obtain a simplified reservoir model. As shown in Figure 2, large-scale fractures are assumed to be main fluid conduits and to have a big impact on flow pattern. For this reason, large-scale fractures are kept explicitly in the EDFM to model them with great accuracy. Medium-scale fracture lengths are about one to five times of the grid size and are modeled by the dual-porosity model. Small-scale fractures are expected to have a small impact on flow field. These fractures are approximated by effective “damaged matrix rock” properties, which are obtained by upscaling methods. This way, the small and medium fractures are deducted from the EDFM, resulting in a big reduction in the simulation effort.

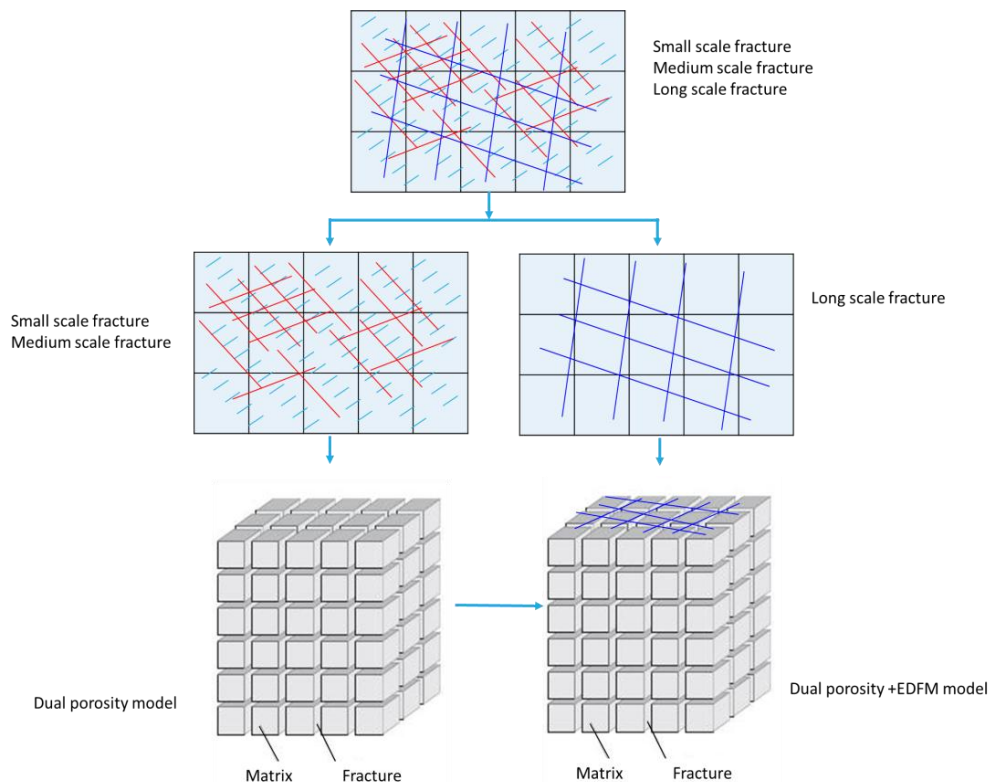


Figure 2. The process to build dual porosity dual permeability (DPDP) model and embedded discrete fracture +DPDP model (EDFM+DPDP).

The key aspect of the new model is the calculation of connection transmissibility for flux interaction among different continua. Non-neighboring connections (NNCs) are subsequently determined as

adding cells to represent fracture segments. Figure 3 illustrates the connection list of continua in the computational domain for a simple scenario. We adopted and extended the definition of NNCs, Four types of NNCs, which were adopted and extended from Moïfar [20], are defined as follows:

NNC type I: connection between a fracture segment and the fracture cell in the dual-porosity model;

NNC type II: connection between fracture segments in an individual fracture;

NNC type III: connection between intersecting fracture segments;

NNC type IV: connection between a fracture segment and the matrix cell in the dual-porosity model.

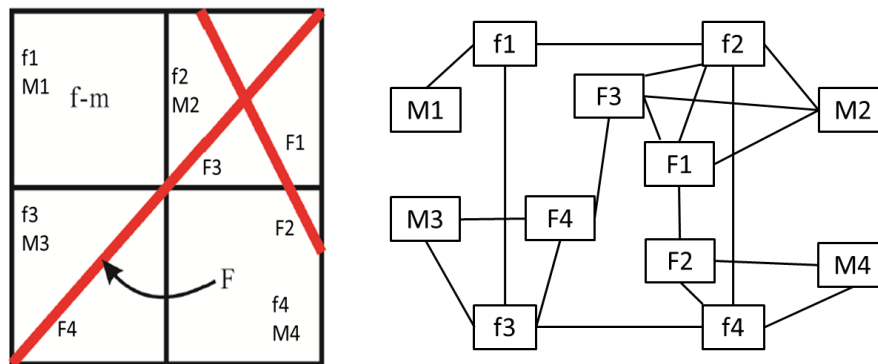


Figure 3. The example of connection list for EDFM+DP method.

2.1. NNC Type I: Connection between a Fracture Segment and the Fracture Cell in the Dual-Porosity Model

The NNC transmissibility factor between the fracture segment and fracture cell in the dual-porosity model depends on the fracture geometry and fracture permeability. As a fracture segment fully penetrates a matrix cell, the fracture–fracture cell transmissibility factor is:

$$T_{f-f_e} = \frac{k_{ff_e} A_{ff_e}}{d_{f-f_e}} \tag{1}$$

where A_{ff_e} is the area of the fracture segment on one side and k_{ff_e} is the permeability tensor, which is calculated as:

$$k_{ff_e} = \frac{2 \times k_{f_e} k_f}{k_f + k_{f_e}} \tag{2}$$

k_f is the embedded fracture permeability tensor, k_{f_e} is the fracture cell permeability tensor, and d_{f-f_e} is the average normal distance from fracture to embedded fracture, which is calculated as:

$$d_{f-f_e} = \frac{\int_v x_n dV}{V} \tag{3}$$

where V is the volume of the fracture cell, dV is the volume element of matrix, and x_n is the distance from the volume element to the fracture plane.

2.2. NNC Type II: Connection between Fracture Segments in an Individual Fracture

The transmissibility factor between a pair of neighboring segments 1 and 2 is calculated using a two-point flux approximation scheme as:

$$T_{feifej} = \frac{2 \times T_{fei} T_{fej}}{T_{fei} + T_{fej}} \tag{4}$$

$$T_{fei} = \frac{k_{fei} A_c}{d_{seg1}} \tag{5}$$

$$T_{fej} = \frac{k_{fej}A_c}{d_{seg2}} \quad (6)$$

where k_{fei} and k_{fej} are the fracture permeability, A_c is the area of the common face for these two segments, and d_{seg1} and d_{seg2} are the distances from the centroids of segments 1 and 2 to the common face, respectively.

2.3. NNC Type III: Connection between Intersecting Fracture Segments

It is very challenging to model fracture intersection accurately and efficiently for DFM due to the complexity of flow behavior at the fracture intersection. In 2014, Moinfar et al. [9] simplified this problem. They approximated the mass transfer at the fracture intersection by assigning a transmissibility factor between intersecting fracture segments. The transmissibility factor is given as:

$$T_{int} = \frac{2 \times T_1 T_2}{T_1 + T_2} \quad (7)$$

$$T_1 = \frac{k_{f1} \omega_{f1} L_{int}}{d_{f1}} \quad (8)$$

$$T_2 = \frac{k_{f2} \omega_{f2} L_{int}}{d_{f2}} \quad (9)$$

where L_{int} is the length of the intersection line and d_{f1} and d_{f2} are the weighted average of the normal distances from the centroids of the subsegments (on both sides) to the intersection line.

2.4. NNC Type IV: Connection between a Fracture Segment and the Matrix Cell in the Dual-Porosity Model

The matrix permeability and fracture geometry determine the NNC transmissibility factor between matrix and fracture segment. When a matrix cell is fully penetrated by a fracture segment, the matrix-fracture transmissibility factor is:

$$T_{f-m} = \frac{k_{mfe} A_{mfe}}{d_{f-m}} \quad (10)$$

where A_{mfe} is the area of the fracture segment on one side and k_{mfe} is the permeability tensor, which is calculated as:

$$k_{mfe} = \frac{2 \times k_{fe} k_m}{k_f + k_m} \quad (11)$$

k_{fe} is the fracture permeability tensor, k_m is the matrix permeability tensor, and d_{f-m} is the average normal distance from matrix to fracture, which is calculated as:

$$d_{f-m} = \frac{\int_v x_n dV}{V} \quad (12)$$

where V is the volume of the matrix cell, dV is the volume element of matrix, and x_n is the distance from the volume element to the fracture plane.

If the fracture does not fully penetrate the matrix cell, the pressure distribution in the matrix cell may deviate from previous assumptions. As a result, the calculation of the transmissibility factor is complex. To make the method non-intrusive, it was assumed the transmissibility factor is proportional to the area of the fracture segment inside of the matrix cell.

3. Model Validation

As mentioned by Tene et al. [17], using EDFM for fractures with very low permeability may create inaccurate results. So only permeable fractures are considered in this study. In this section, we present

a three-dimensional (3D) case with two sets of permeable fractures. The hybrid EDFM-DPDP approach is compared to EDFM, DFM, and dual-porosity approaches to verify the accuracy of the hybrid EDFM-DPDP method in modeling fracture networks. Figure 4 shows the dimensions of the reservoir and the positions of fracture planes. Figure 4a shows the fracture system used in this study. Figure 4b is the DFM with 213,810 cells. Figure 4c is the DPDP model, with a flow-based method used to homogenize all of the fractures in the upscaling process. Figure 4d is the EDFM, explicitly showing the fractures. Figure 4e shows the hybrid EDFM-DPDP method, picturing one set of fractures by dual porosity and the other set of fractures by EDFM. In the hybrid EDFM-DPDP method, small- and medium-scale fractures are upscaled by a flow-based method.

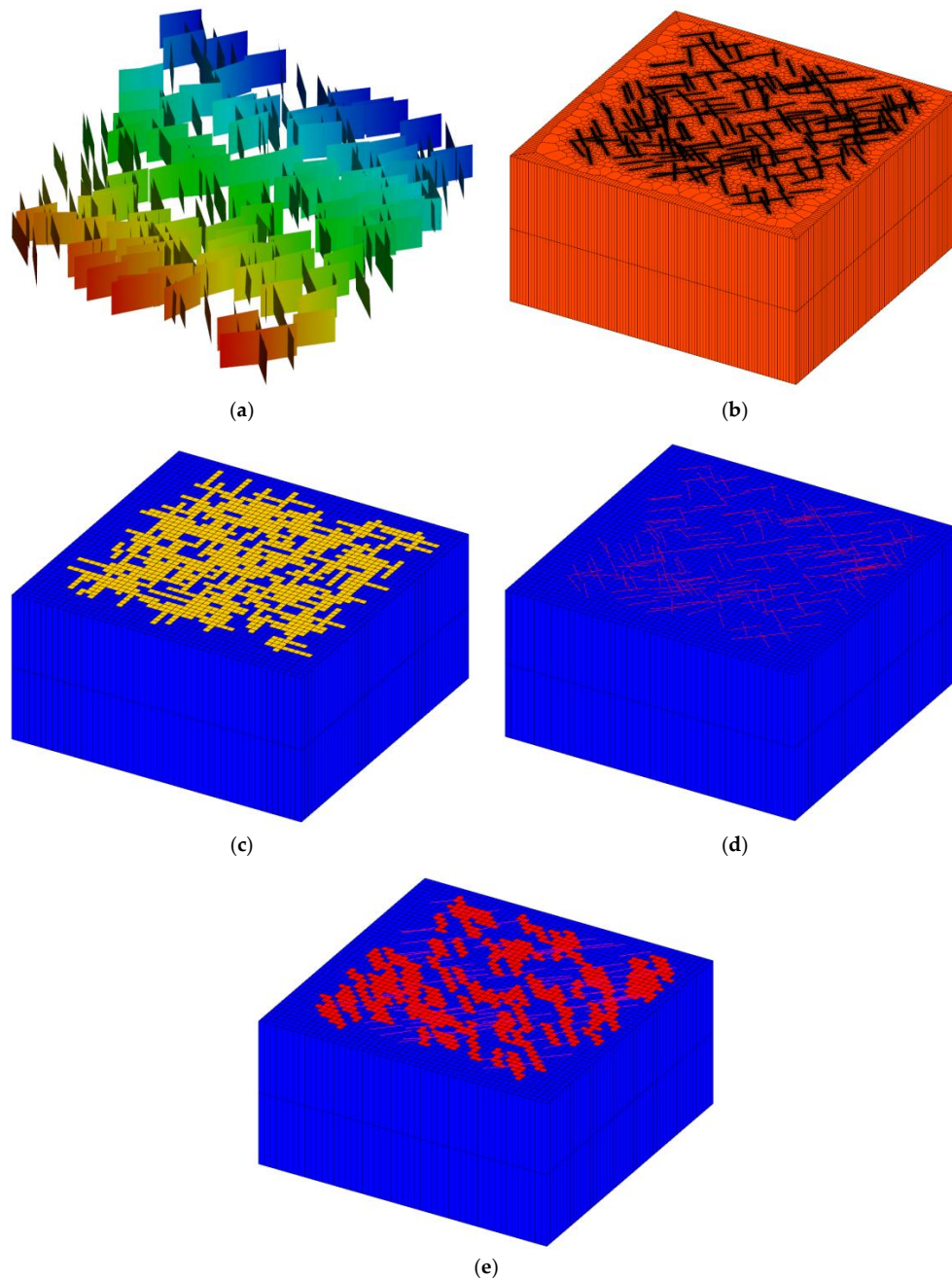


Figure 4. Fracture model. (a) Fracture model; (b) DFM; (c) Dual-porosity model; (d) EDFM; and, (e) hybrid EDFM-DPDP method.

The reservoir dimensions are $1000 \times 1000 \times 20$ ft. The fractures fully penetrate the reservoir vertically (with a height of 20 ft from the top to the bottom of the reservoir). The width and permeability of the fractures is 0.01 ft and 500 md, respectively. As a result, the fracture conductivity is 5 md-ft. A uniform $50 \times 50 \times 2$ matrix grid is defined in dual-porosity, EDFM, and hybrid EDFM-DPDP methods. The dimensions of the matrix cells are $20 \times 20 \times 10$ ft. Five vertical wells are defined in the reservoir: one is a water injector located at the reservoir center, with an injection rate of 200 stb/day and limited bottomhole pressure (BHP) no more than 5000 psi; the other four wells are oil producers located at the corner, with oil rates of 50 stb/day and limited BHP no less than 500 psi.

This example is for water injection of a low-permeability oil reservoir. The reservoir is isotropic as the permeabilities in the X, Y, and Z directions are the same. The Corey model was used for the relative permeability curve for both matrix and fracture. Peaceman's model was applied to calculate the well indices. The detailed reservoir and fluid properties are summarized in Table 1.

Table 1. Reservoir and Fluid Properties.

Parameter	Value
Matrix permeability K_x (md)	0.001
Matrix permeability K_y (md)	0.001
Matrix permeability K_z (md)	0.001
Reservoir porosity	0.05
Reservoir pressure (psi)	3000
Reservoir temperature ($^{\circ}$ F)	150
Oil viscosity (mPa·s)	0.98
Water viscosity (mPa·s)	0.50

Figure 5 shows the well oil production rates and the cumulative oil production of different models. The results of EDFM and DFM are highly consistent in these plots, and the dual-porosity model is significantly different among these methods, while curves from the hybrid EDFM-DPDP method are between that from dual-porosity and DFM methods, indicating that EDFM improves the accuracy and verifying of the the EDFM. The upscaling method and grid refinement are considered as other ways to improve accuracy of the dual-porosity model. In this study, we also run five cases with different upscaling methods (Oda method and flow-based method with different boundaries: linear, constant pressure, no-flow, and periodic) and three cases with different grid sizes from 5 to 20 for dual porosity. The comparison among different upscaling methods with the EDFM method is shown in Figure 6. Figure 6a indicates that different upscaling methods reach similar results for water flooding, and Figure 6b shows the difference between the Oda method and other upscaling methods for gas flooding. Meanwhile, the figure also shows a significant difference between these upscaling methods and EDFM.

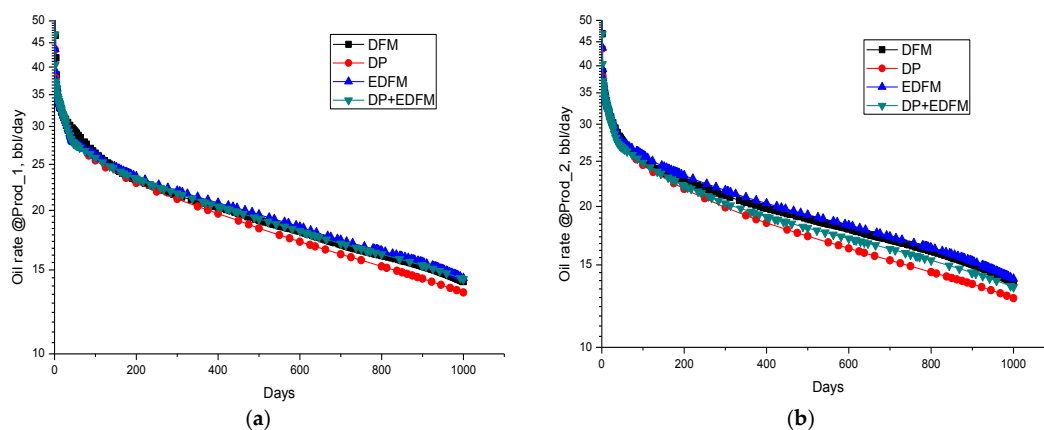


Figure 5. Cont.

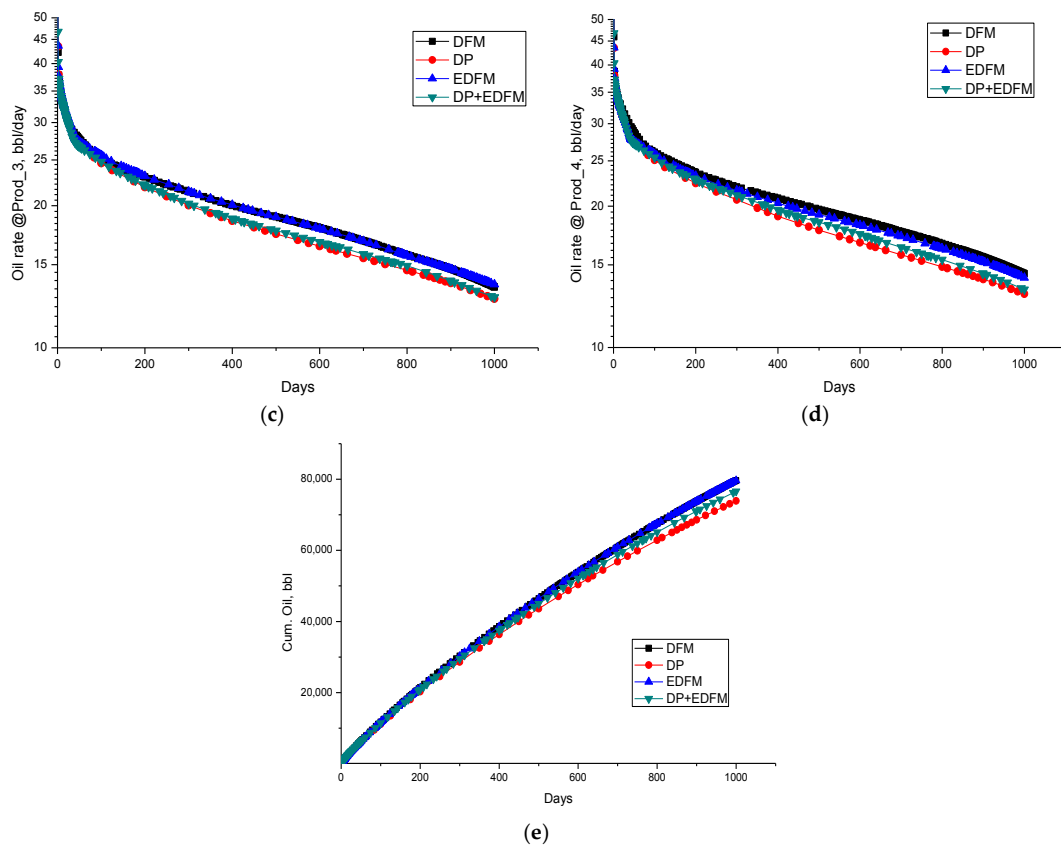


Figure 5. Comparison of production for different models. (a) Well “Prod_1” oil rate; (b) Well “Prod_2” oil rate; (c) Well “Prod_3” oil rate; (d) Well “Prod_4” oil rate; and, (e) Field cumulative oil.

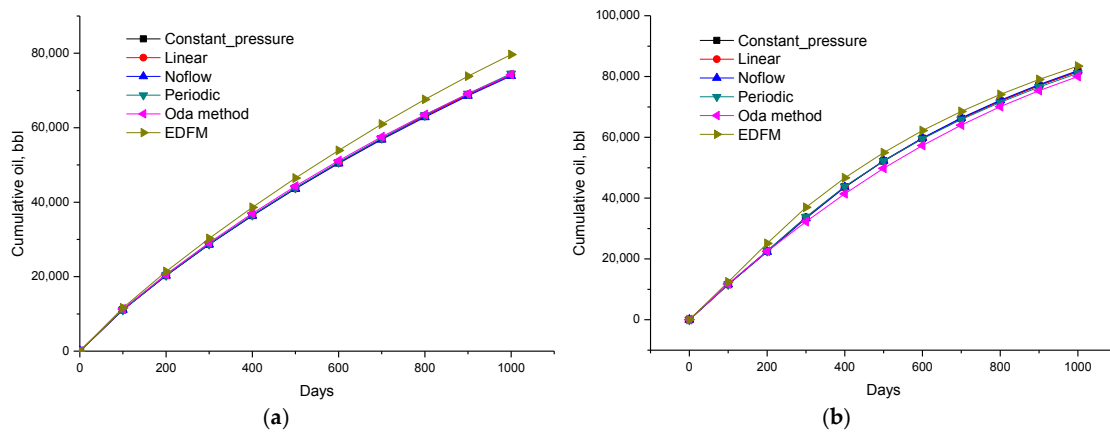


Figure 6. Simulation results for different models. (a) water flooding; (b) gas flooding.

Capillary pressure plays an important role in fractured reservoir. In this study, different methods with capillary pressure for water flooding are studied. As shown in Figure 7, the difference between EDFM and DP methods is about 3.5–4.0%. While the difference is 1.5% between EDFM and hybrid EDFM and DP methods.

Figure 8 shows the cumulative oil and time consumption vs. different models. We can find that the refinement grid from 20 to 5 m for the dual-porosity model doesn't improve accuracy in this study, and time consumption increases from 25 to 2927 s when grid number increases from 5000 to 16,000 in the DP models. The figure also points out that DFM consumes 4322 s, EDFM takes 268 seconds, and the hybrid EDFM-DPDP method takes 55 s. All of the simulations were performed on a 2.6 GHz, Intel

CoreDuo CPU. The time consumption of the hybrid EDFM-DPDP method is only 1/80 that of the DFM method and 1/5 that of the EDFM method. From the study, we conclude that EDFM maintains accuracy and saves CPU time.

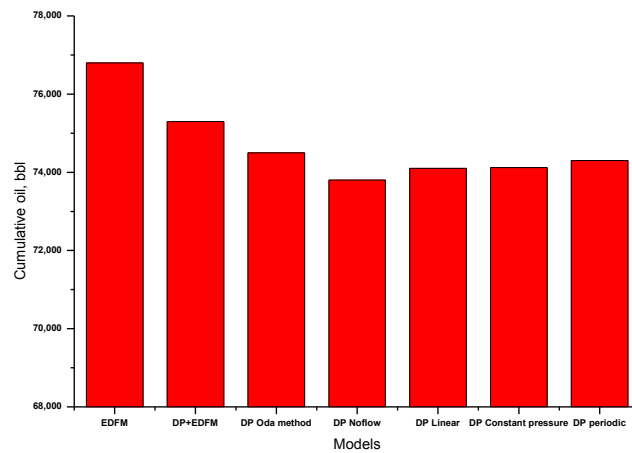
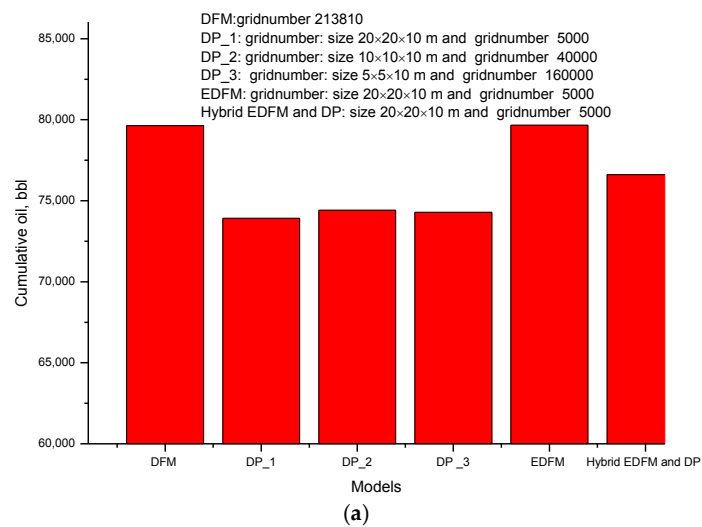
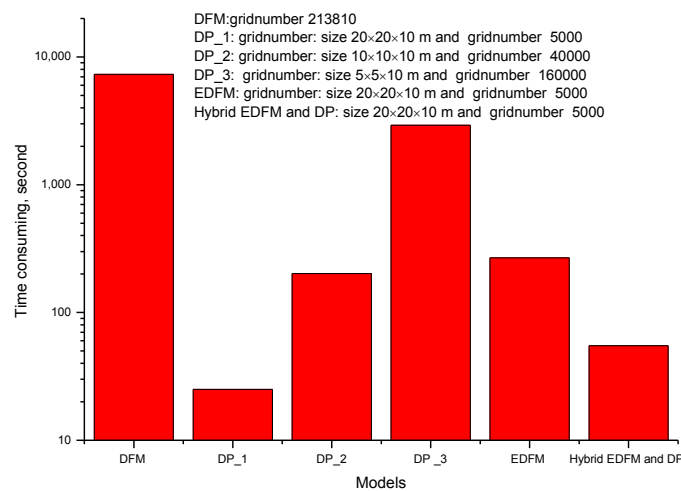


Figure 7. Simulation results for different models with capillary pressure for water flooding.



(a)



(b)

Figure 8. Simulation results for different models. (a) Cumulative oil for different models; (b) Time consumption for different models.

4. Comprehensive Sensitivity Studies

There is high uncertainty in shale oil formations because of many uncertain parameters, such as reservoir permeability, fracture half-length, number of fractures, and fracture conductivity. In addition, parameters related to CO₂ huff-and-puff are also uncertain, such as CO₂ injection rate, injection time, and soaking time, and the number of cycles of CO₂ huff-and-puff. Accordingly, in the subsequent simulation study, we perform a series of simulations to investigate the impacts of these uncertain parameters related to the CO₂ huff-and-puff process.

4.1. Reservoir Model

As shown in Figure 9, a base model is constructed to perform simulation studies for a single horizontal well with natural fractures and multiple hydraulic fractures in a shale oil reservoir. Several reservoir and fracture parameters are analyzed, including natural fracture permeability, hydraulic fracture permeability, hydraulic fracture half-length, hydraulic fracture stages, and so on.

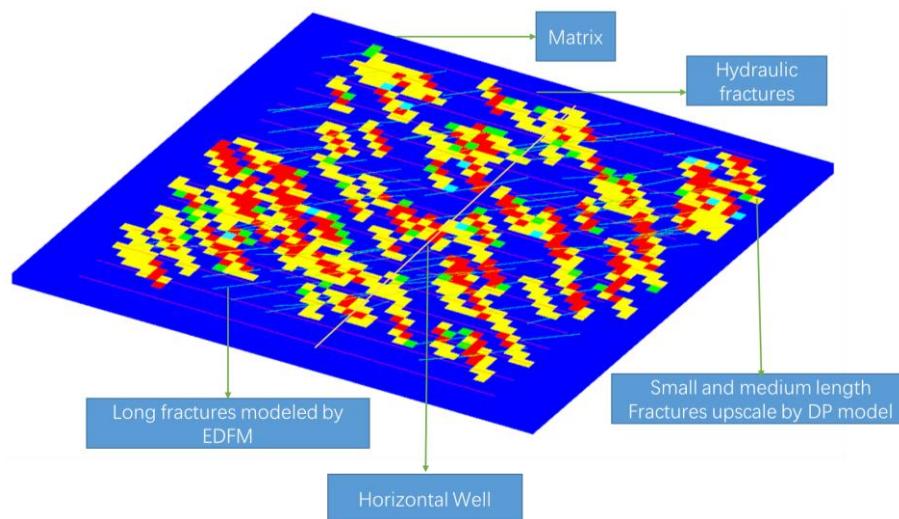


Figure 9. Natural fracture, hydraulic fracture distribution in reservoir.

The parameters assumed for the model are summarized in Table 2. The properties of the components used for the simulation studies are shown in Table 3.

Table 2. Parameters of the base model.

Parameters	Values
Reservoir Dimensions (x, y, z), ft	1000, 1000, 20
Gridblock size (x, y, z), ft	20, 20, 10
Initial reservoir pressure, psi	5000
Temperature, F	150
Matrix porosity	0.05
Fracture porosity	0.01
Fracture half length, ft	400
Short-medium natural fracture permeability, md	0.02
Large natural fracture permeability, md	0.02
Large natural fracture number	108
Hydraulic fracture permeability, md	2.00
Matrix permeability, md	0.001
Hydraulic fracture number	16
Producer BHP, psi	4000
Injection BHP, psi	6000

Table 3. Live oil composition and properties.

Component	Mole Fraction, %	Critical Pressure, psi	Critical Temperature, °R	Acentric Factor	Molecular Weight, g/mol
CO ₂	0.01	1055.88	547.56	0.23	44.01
CH ₄	0.24	667.2	343.08	0.01	16.04
C2–C4	0.22	497.47	1007.532	0.25	95.33
C5–C6	0.23	347.6	1068.05	0.4	124.12
C7–C11	0.18	248.97	1212.01	0.62	181.06
C12+	0.12	136.43	700.45	1	259.99

In huff-and-puff recovery, we maintain injection pressure to be higher than the minimum miscibility pressure. In this study, the minimum miscibility pressure is estimated to be 3000 psi based on experiment and slim-tube simulation. Therefore, well BHP is set to 4000 psi during production and well BHP is set to 6000 psi during the CO₂ injection. During the injection process, pure CO₂ is injected into the reservoir. Specifically, the well pressure is fixed at 4000 psi from day 1 to 300 to carry out primary recovery. Then, the well is operated as an injection well from day 301 to 360 at a fixed pressure of 4000 psi. During this period, pure CO₂ is injected into the reservoir. From day 361 to 390, the well is closed, letting the CO₂ mix with oil in the reservoir. From day 391 to 480, the well is reopened to produce hydrocarbons at a fixed pressure of 4000 psi. The same CO₂ huff-and-puff steps are repeated until day 1200, giving rise to five cycles of CO₂ huff-and-puff. Detailed steps are listed in Table 4.

Table 4. CO₂ huff-and-puff steps.

Step 1	Step 2	Step 3	Step 4	Step 5
300 days of primary recovery; production pressure = 4000 psi	60 days of CO ₂ injection; injection pressure = 6000 psi	30 days of well shut-in	90 days of production; production pressure = 6000 psi	Repeat steps 2 to 4 until 1200 days

4.2. Large Natural Fracture Permeability

A sensitivity study was conducted on large natural fracture permeability for 0.02, 0.2, and 2 md with 16 hydraulic fractures. Figure 10a shows that the oil rate depletes from 40 to 2.4 m³/day for the first 300 days, with primary recovery being only 0.62%. After 60 days of gas injection and 10 days of soaking, oil rate increases to 40 m³/day and decreases to 7 m³/day at the end of the first cycle. Figure 10b shows the oil recovery increase from 3.51 to 3.95% when natural fracture permeability increases from 0.02 to 2.0 md, which means a 12.5% improvement. The results illustrate that using gas huff-and-puff could significantly improve production and remarkably impact the permeability of the cumulative oil production. Higher natural fracture permeability can provide higher flow conductivity and result in higher oil recovery.

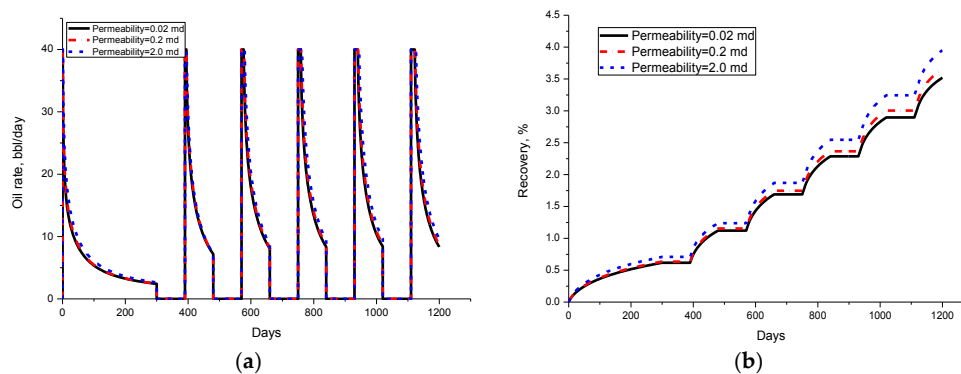


Figure 10. Simulation results for different natural fracture permeabilities. (a) Oil rate of different natural fracture permeabilities; (b) Recovery of different natural fracture permeabilities.

4.3. Hydraulic Fracture Permeability, Length, and Stages

A simulation study is performed on hydraulic fracture permeability for 2, 20, 100, 500, and 5000 md, with natural fracture permeability of 0.02 md, number of hydraulic stages of 16, and a half-length of 400 ft. Figure 11 shows the simulation results of five different hydraulic fracture permeabilities. The Figure illustrates that a higher hydraulic fracture permeability results in a higher recovery. Oil recovery increases from 3.51 to 4.51% when hydraulic fracture permeability increases from 2 to 100 md. However, oil recovery only increases 0.20% when permeability increases from 100 to 5000 md. The results illustrate that there exists an optimum value of hydraulic fracture permeability. Over the optimum value (100 md in this case), increasing hydraulic fracture permeability has a slight impact on oil recovery.

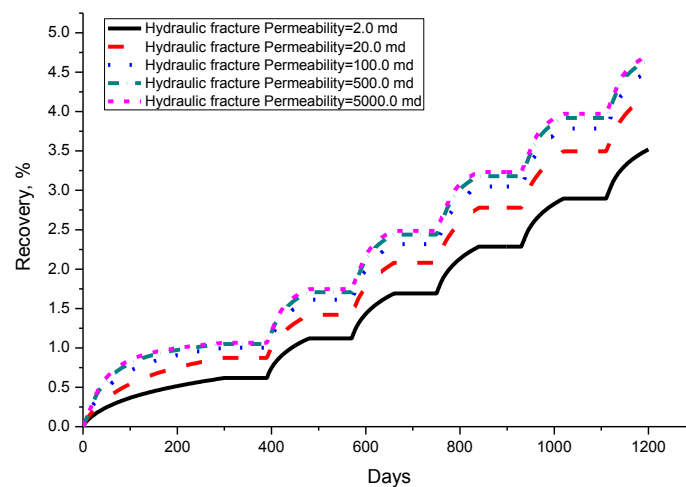


Figure 11. Recovery of different hydraulic fracture permeabilities.

A comparison of oil recovery factor with different hydraulic fracture lengths is shown in Figure 12. In this study, half-hydraulic-fracture-lengths for three cases are 200, 300, and 400 m. In the Figure, we can find that more oil can be produced with a longer hydraulic fracture. This is because longer hydraulic fractures yield more connections with natural fractures and matrix, resulting in higher oil recovery.

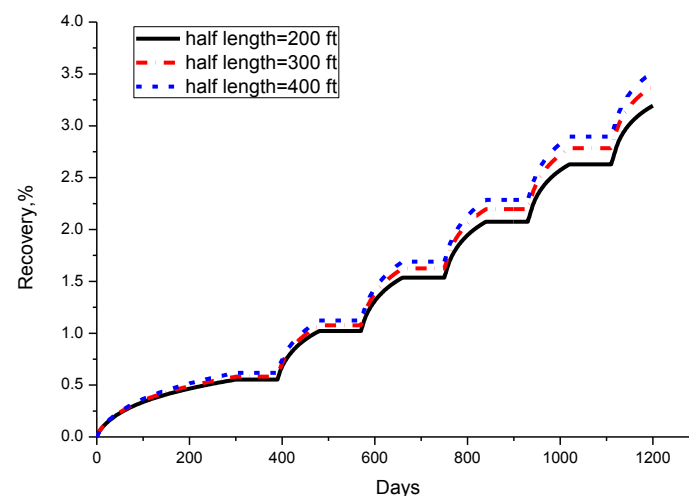


Figure 12. Recovery of different hydraulic fracture lengths.

The hydraulic fracture stage is one important parameter with a significant impact on the CO₂ huff-and-puff process in shale oil. In this case, we run five cases with different numbers of stages from 8 to 24. Figure 13 shows the recovery and oil rate vs. time at different fracture stages. When the stage increases from 8 to 24, oil recovery increases from 2.70 to 3.90%, which means recovery improved by 44% for the case at stage number 8.

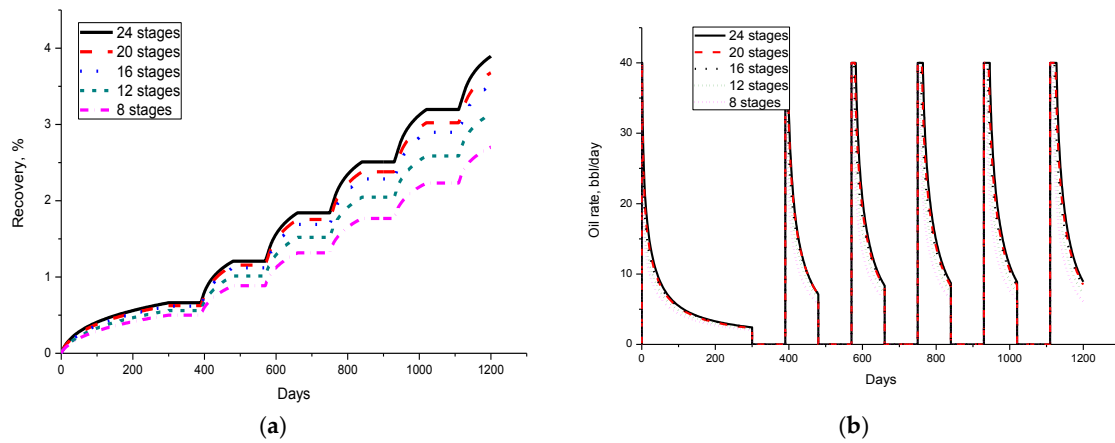


Figure 13. Simulation results for different hydraulic fracture stages. (a) Recovery of different hydraulic fracture stages; (b) Oil rate of different hydraulic fracture stages.

4.4. Capillary Pressure

Capillary pressure is one of the important parameters for fractured reservoir, especially when water flooding and gas flooding processes are involved. In this study, we run three cases with different capillary pressure curves. Figure 14a shows capillary pressure curves used in the study and Figure 14b shows the recovery for different curves. Recovery decreases with capillary pressure increases, and the case without capillary pressure reach higher recovery.

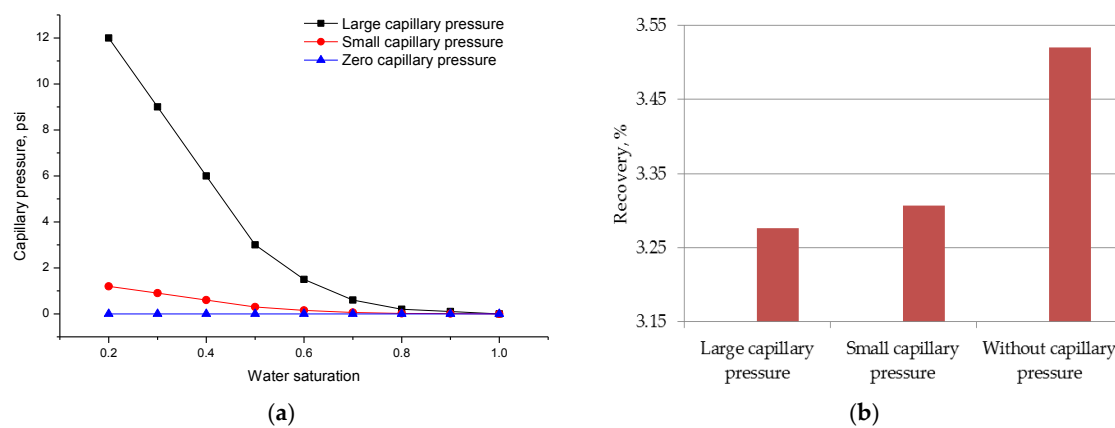


Figure 14. Simulation results for different capillary pressure. (a) Three capillary pressure curves (b) Recovery of different capillary pressure curves.

4.5. Huff-And-Puff Scenario

In order to investigate the effect of the huff-and-puff scenario on the CO₂ estimated oil recovery (EOR) process, several parameters are modified from the base model set up previously (the others remain unchanged). We compare three cases to determine the better injection strategy for the huff-and-puff scenario. The huff-and-puff patterns are summarized in Table 5. We fix the total production and injection periods with different combinations. Figure 15 shows the impact of different

strategies on cumulative oil production. The Figure also shows that a reduced cycle length and increased cycles could increase the oil production.

Table 5. Simulation patterns.

	Injection Days	Soaking Days	Production Days	Cycles
Case_1	60	30	90	5
Case_2	100	50	150	3
Case_3	30	15	45	10

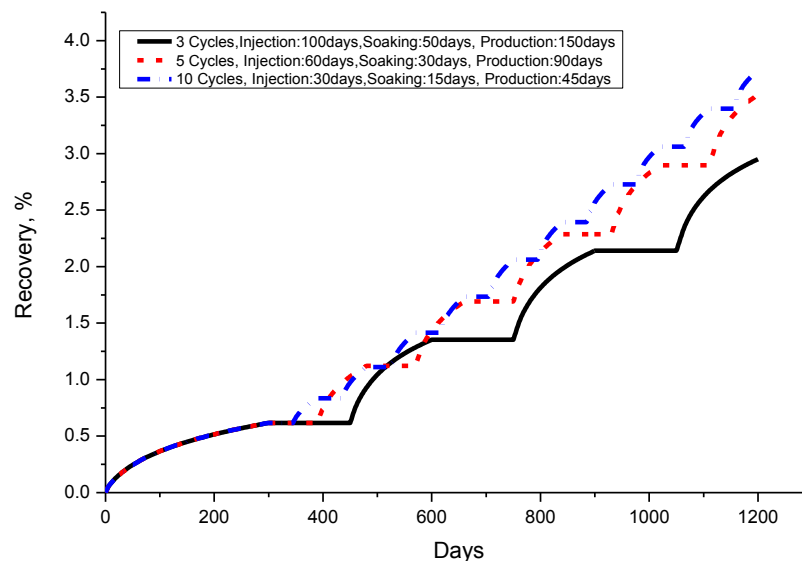


Figure 15. Cumulative oil production of different injection pattern times.

5. Conclusions

In this work, we implement a novel simulation method that integrates EDFM and dual-continuum methods to successfully simulate a complex fracture network with multiple orientations and length-scales induced by hydraulic fracturing treatment. The hybrid model could explicitly describe the dominant role of large-scale fractures on flow conduits, as well as offer computationally efficient simulations without employing unstructured gridding and mesh refinement near fractures. The small and medium natural fracture networks connecting the global flow are simulated by the dual-continuum model. The proposed numerical model is designed and compared with DFM, EDFM, and dual-porosity methods, and comprehensive modeling studies are conducted to understand the key reservoir and fracture properties that affect production performance and to investigate the feasibility of CO₂ huff-and-puff in shale oil reservoirs. We obtain the following conclusions from the simulation results:

- (1) The study verifies that this new EDFM-DPDP method can save time and maintain high accuracy.
- (2) Increasing hydraulic fracture permeability and enhancing hydraulic fracture intersection with an extensive network of natural fractures is the key to improving well productivity.
- (3) Incremental oil is sensitive to natural fracture permeability, hydraulic fracture permeability, number of stages, cycling length, and number of cycles.

Acknowledgments: The authors are grateful for financial support from the State Major Science and Technology Special Project of China during the 13th Five-Year Plan (Grant No. 2016ZX05014-004, 2016ZX05025-003-007 and 2016ZX05034-001-007) and Major Project of China National Petroleum Corporation (Grant No. RIPED-2017-JS-236).

Author Contributions: Weirong Li and Zhenzhen Dong conceived of the presented idea. Weirong Li developed the theory and performed the computations. Zhenzhen Dong and Gang Lei verified the methods. Zhenzhen Dong

encouraged Weirong Li to investigate CO₂ Huff and Puff in shale oil with new model and supervised the findings of this work. All authors discussed the results and contributed to the final manuscript.

Conflicts of Interest: There are no conflicts of interest.

References

1. Snow, D.T. The frequency and apertures of fractures in rock. *Int. J. Rock Mech. Min. Sci. Geomech. Abstr.* **1970**, *7*, 23–30. [[CrossRef](#)]
2. Oda, M. An equivalent continuum model for coupled stress and fluid flow analysis in jointed rock masses. *Water Resour. Res.* **1986**, *22*, 1845–1856. [[CrossRef](#)]
3. Tian, K. The discussion on hydrogeology model of fractured rock. *Site Investig. Sci. Technol.* **1984**, *4*, 27–34.
4. Barenblatt, G.I.; Zheltov, I.P.; Kochina, I.N. Basic concepts in the theory of seepage of homogeneous liquids in fissured rocks. *J. Appl. Math. Mech.* **1960**, *24*, 1286–1303. [[CrossRef](#)]
5. Warren, J.E.; Root, P.J. The behavior of naturally fractured reservoirs. *Soc. Pet. Eng. J.* **1963**, *3*, 245–255. [[CrossRef](#)]
6. Kazemi, H.; Merrill, L.S., Jr.; Porterfield, K.L.; Zeman, P.R. Numerical simulation of water-oil flow in naturally fractured reservoirs. *Soc. Pet. Eng. J.* **1976**, *16*, 317–326. [[CrossRef](#)]
7. Saidi, A.M. Simulation of Naturally Fractured Reservoirs. In Proceedings of the SPE Reservoir Simulation Symposium, San Francisco, CA, USA, 15–18 November 1983.
8. Pruess, K.; Narasimhan, N.T. A practical method for modeling fluid and heat flow in fractured porous media. *Soc. Pet. Eng. J.* **1985**, *25*, 14–26. [[CrossRef](#)]
9. Moinfar, A.; Varavei, A.; Sepehrnoori, K.; Johns, R.T. Development of a novel and computationally efficient discrete-fracture model to study IOR processes in naturally fractured reservoirs. In Proceedings of the SPE Improved Oil Recovery Symposium, Tulsa, OK, USA, 14–18 April 2012.
10. Kim, J.; Deo, M.D. Finite element, discrete-fracture model for multiphase flow in porous media. *AIChE J.* **2000**, *46*, 1120–1130. [[CrossRef](#)]
11. Karimi-Fard, M.; Firoozabadi, A. Numerical simulation of water injection in fractured media using the discrete fractured model and the Galerkin method. *SPE Reserv. Eval. Eng.* **2003**, *6*, 117–126. [[CrossRef](#)]
12. Monteagudo, J.E.P.; Firoozabadi, A. Control-volume model for simulation of water injection in fractured media: Incorporating matrix heterogeneity and reservoir wettability effects. *SPE J.* **2007**, *12*, 355–366. [[CrossRef](#)]
13. Matthäi, S.K.; Belayneh, M. Fluid flow partitioning between fractures and a permeable rock matrix. *Geophys. Res. Lett.* **2004**, *31*, L07111. [[CrossRef](#)]
14. Karimi-Fard, M.; Durlofsky, L.J.; Aziz, K. An efficient discrete-fracture model applicable for general-purpose reservoir simulators. *SPE J.* **2004**, *9*, 227–236. [[CrossRef](#)]
15. Li, L.; Lee, S.H. Efficient field-scale simulation of black oil in a naturally fractured reservoir through discrete fracture networks and homogenized media. *SPE Reserv. Eval. Eng.* **2008**, *11*, 750–758. [[CrossRef](#)]
16. Hajibeygi, H.; Karvounis, D.; Jenny, P. A hierarchical fracture model for the iterative multiscale finite. *J. Comput. Phys.* **2017**, *230*, 8729–8743. [[CrossRef](#)]
17. Tene, M.; Sebastian, B.M.B.; Al Kobaisi, M.S.; Hajibeygi, H. Projection-based embedded discrete fracture model (pEDFM). *Adv. Water Resour.* **2017**, *105*, 205–216. [[CrossRef](#)]
18. Zidane, A.; Firoozabadi, A. Fracture-cross-flow equilibrium in compositional two-phase reservoir simulation. *SPE J.* **2017**, *22*, 950–970. [[CrossRef](#)]
19. Plumers, S. Hierarchical Fracture Modeling Approach. Master's Thesis, Delft University of Technology, Delft, The Netherlands, 2015.
20. Moinfar, A. Development of an Efficient Embedded Discrete Fracture Model for 3D Compositional Reservoir Simulation in Fractured Reservoirs. Doctor of Philosophy's Dissertation, The University of Texas at Austin, Austin, TX, USA, 2013.

